PHYSICAL REVIEW D **84,** 115008 (2011)

Spin analysis of *s*-channel diphoton resonances at the LHC

M. C. Kumar,[1,*] Prakash Mathews,[2,†] A. A. Pankov,[3,‡] N. Paver,[4,§] V. Ravindran,[5,‖] and A. V. Tsytrinov[3,¶]

[1]*Deutsches Elektronen-Synchrotron DESY, Platanenallee 6, D-15738 Zeuthen, Germany*
[2]*Saha Institute of Nuclear Physics, 1/AF Bidhan Nagar, Kolkata 700064, India*
[3]*The Abdus Salam ICTP Affiliated Centre, Technical University of Gomel, 246746 Gomel, Belarus*
[4]*University of Trieste and INFN-Trieste Section, 34100 Trieste, Italy*
[5]*Regional Centre for Accelerator-based Particle Physics, Harish-Chandra Research Institute, Chhatnag Road, Jhunsi, Allahabad 211 019, India*

(Received 25 August 2011; published 8 December 2011; publisher error corrected 21 December 2011)

The high mass neutral quantum states envisaged by theories of physics beyond the standard model can, at the hadron colliders, reveal themselves through their decay into a pair of photons. Once such a peak in the diphoton invariant mass distribution is discovered, the determination of its spin through the distinctive photon angular distributions is needed in order to identify the associated nonstandard dynamics. We discuss here the discrimination of the spin-2 Randall-Sundrum graviton excitation against the hypothesis of a spin-0 exchange giving the same number of events under the peak, by means of the angular analysis applied to resonant diphoton events expected to be observed at the LHC. The spin-0 hypothesis is modeled by an effective interaction of a high mass gauge singlet scalar particle interacting with the standard model fields. The basic observable of our analysis is the symmetrically integrated angular asymmetry A_{CE}, calculated for both graviton and scalar *s*-channel exchanges to next-to-leading order in QCD.

DOI: 10.1103/PhysRevD.84.115008 PACS numbers: 12.60.−i, 11.10.Kk, 12.60.Cn

I. INTRODUCTION

Diphoton final states represent a very important testing ground for the standard model (SM); for example, they may be one of the main discovery channels for the Higgs boson searches at the CERN LHC. Moreover, similar to the case of dileptons, the inclusive production of two-photon high mass resonance states at the LHC,

$$p + p \to \gamma\gamma + X, \tag{1}$$

is considered as a powerful, clean test of new physics (NP), would an excess of $\gamma\gamma$ events be observed with respect to the prediction from the SM cross section.

One NP scenario of particular importance is the case of the spin-2 Kaluza-Klein (KK) graviton excitations predicted by the Randall-Sundrum (RS) model of gravity in one warped spatial extra dimension [1]. This model suggests a rich phenomenology that includes the production of diphoton resonances, to be explored at collider energies; see, for example, Refs. [2–4]. The existence of such graviton excitations can be signaled by the occurrence of peaks in the invariant mass distribution of the photon pairs, and, indeed, the lowest-lying predicted diphoton peak has recently been searched for in experiments at the $p\bar{p}$ Fermilab Tevatron collider [5,6], and at the 7 TeV pp LHC collider with time-integrated luminosity of the order of 40 pb^{-1} [7,8]. In these experiments, exclusion mass limits on the lightest RS resonance of the TeV order have been set, and graviton mass scales larger than 1 TeV will certainly be in the kinematical reach of the LHC.

Assuming that a diphoton peak at an invariant mass value M_R is observed, its association to a specific NP scenario would be possible only if we are able to discard other competing models, potential sources of the peak itself with the same M_R and the same number of events. Basically, for any nonstandard model one can define, on the basis of the foreseeable statistics and uncertainties, a discovery reach on the relevant heavy resonance R as the upper limit of the range in M_R where, in a specific domain of the model parameters called ''signature space,'' the peak is expected to give a signal observable over the SM prediction to a prescribed confidence level. Instead, the identification reach on the model is the upper limit of the range in M_R where it can be identified as the source of the peak, once discovered, or, equivalently, the other competing models can be excluded for all values of their respective parameters. Of course, for many models, identification should be possible only in a subdomain of their signature space.

The determination of the spin of an observed resonance clearly represents an important selection among different classes of nonstandard interactions. In the case of the inclusive diphoton production (1), the tool to directly test the spin-2 of the RS graviton resonance or, equivalently, exclude the hypothesis of a spin-0 scalar particle exchange would be provided by the distinctive angular distributions in the angle θ between the incident quark or gluon and the final photon in the diphoton center-of-mass frame. This is similar to dilepton production, the difference being that in

*kumar.meduri@desy.de
†prakash.mathews@saha.ac.in
‡pankov@ictp.it
§nello.paver@ts.infn.it
‖ravindra@hri.res.in
¶tsytrin@rambler.ru

 © 2011 American Physical Society

this case the hypotheses of both the spin-0 and the spin-1 exchanges must simultaneously be excluded.

The spin-2 test of the lowest-lying RS graviton in lepton-pair collider events, through the direct comparison of the angular distributions for the various spin hypotheses, was discussed earlier in several papers (see, e.g., Refs. [9–11]), and experimental angular analyses were attempted at the Tevatron in Ref. [12]. A potential difficulty of the direct-fit angular analysis at the LHC is that generally, due to the symmetry of the proton-proton initial configuration, the determination on an event-by-event basis of the direction of the initial parton, hence of the sign of $\cos\theta$, is, in principle, not fully unambiguous, so cuts in phase space must be applied in this regard.

The spin-2 RS graviton analysis of LHC dilepton events proposed in Ref. [13] makes use of a ''center-edge'' angular asymmetry $A_{\rm CE}$, where the above-mentioned ambiguity should not be present [14,15]. Essentially, in this observable the dilepton events are weighted according to the $\cos\theta$ differential distributions, and the asymmetry is defined between cross sections symmetrically integrated over ''center'' and ''edge'' angular intervals. Recently, asymmetries conceptually analogous to $A_{\rm CE}$ have been applied to heavy quantum state spin identification in Refs. [16,17], and a comparison of the performances of different methods for heavy resonance identification has been presented in Ref. [18]. Angular analyses for different spin-mediated Drell-Yan processes have been applied to a variety of NP models in Ref. [19].

Here, we propose the application of $A_{\rm CE}$ to the angular analysis of the diphoton production process (1) at the LHC. As remarked previously, the selection of the spin-2 RS graviton amounts, in practice, to excluding the hypothesis of a spin-0 particle exchange with the same mass M_R and producing the same number of diphoton events. Ideally, one advantage of the diphoton channel over dileptons can be represented by the doubled statistics expected in the former case [20]. Also, the automatic exclusion of the spin-1 hypothesis [21,22] should in any case allow a simplification of the analysis from the phenomenological point of view. Finally, the consideration of process (1), in addition to dilepton production, is needed for an exhaustive test of model [1].

For our analysis we have used the calculations of the required differential cross sections to next-to-leading order (NLO) in QCD, and this is essential at a hadron collider as the theoretical uncertainties get reduced when higher order corrections are included. Furthermore, as a result of new interactions in a NP model, there will be additional subprocesses that contribute at LO itself (e.g., $gg \to \gamma\gamma$ in the RS model), and hence the signal can receive enhanced contributions due to the NLO corrections.

Specifically, in Sec. II we review the definitions of the basic cross sections involved in the asymmetry $A_{\rm CE}$; Sec. III will be devoted to the relevant properties and the characteristic angular distributions for the RS graviton and for the competing scalar particle exchanges in process (1), for which we will adopt the model recently proposed in Ref. [23]. In Sec. IV we discuss the NLO QCD effects on the diphoton production rates and on the angular distributions, for both kinds of spin exchange. Section V contains an outline of the $A_{\rm CE}$-based angular analysis and the consequent numerical results for RS identification, in the LHC center-of-mass running configurations $\sqrt{s} = 14$ TeV and $\sqrt{s} = 7$ TeV. Finally, Sec. VI contains some conclusive remarks.

II. CROSS SECTIONS AND CENTER-EDGE ASYMMETRY

The total cross section for a heavy resonance discovery in the events (1) at a diphoton invariant mass $M = M_R$ can be expressed as

$$\sigma(pp \to \gamma\gamma) = \int_{-z_{\rm cut}}^{z_{\rm cut}} dz \int_{M_R-\Delta M/2}^{M_R+\Delta M/2} dM \frac{d\sigma}{dMdz}, \qquad (2)$$

where the rapidity of the individual photon $|\eta_\gamma| < 2.5$ and $z = \cos\theta$ is chosen such that $|z| < 0.98$.

The diagnosis of the resonance spin uses the comparison of the characteristic photon differential distributions for the two hypotheses, spin-2 KK modes of the RS graviton $R = G$ and a massive scalar $R = S$:

$$\frac{d\sigma}{dz} = \int_{M_R-\Delta M/2}^{M_R+\Delta M/2} dM \frac{d\sigma}{dMdz}. \qquad (3)$$

In Eqs. (2) and (3), cuts on the phase space accounting for detector acceptance are implicit, and ΔM is an invariant mass bin around M_R, which should somehow reflect the detector energy resolution and be sufficiently large as to include the resonance width. In the calculations worked out in this article we use, for this mass window, the expression [24]

$$\Delta M = 24(0.625M + M^2 + 0.0056)^{1/2}\ \text{GeV}. \qquad (4)$$

Actually, Eq. (4) was derived in connection to the ATLAS and CMS experiments on dilepton production, but we use it also for the calculations of diphoton production of interest here. Obviously, for a resonance sufficiently narrow, the integral over M should be practically insensitive to the size of ΔM, whereas it should be essentially proportional to ΔM for a flat background such as the SM. Besides $|\eta_\gamma| < 2.5$ mentioned above, the assumed typical cuts on harder (softer) photons are $p_\perp^\gamma > 40\,(25)$ GeV, and the statistics will be estimated by taking a photon reconstruction efficiency $\epsilon_\gamma = 0.80$.

Moreover, to evaluate Eqs. (2) and (3), the partonic cross sections will be convoluted with the CTEQ6L and CTEQ6M parton distribution sets for LO and NLO cross sections, respectively, with $\Lambda_{\rm QCD} = 0.226$ GeV [25]. In particular, for resonance discovery, process (1) must be

observed with a number of events well above the background from SM processes. Specifically, denoting by N_S and $N_{\rm SM}$ the number of signal and SM events in the $\gamma\gamma$ invariant mass window, the statistical significance of a 5σ signal would be ensured by the criterion that N_S should be larger than $\max(5\sqrt{N_{\rm SM}}, 10)$.

The z evenly integrated center-edge angular asymmetry $A_{\rm CE}$ is defined as

$$A_{\rm CE} = \frac{\sigma_{\rm CE}}{\sigma} \text{ with } \sigma_{\rm CE} \equiv \left[\int_{-z^*}^{z^*} - \left(\int_{-z_{\rm cut}}^{-z^*} + \int_{z^*}^{z_{\rm cut}}\right)\right]\frac{d\sigma}{dz}dz. \tag{5}$$

In Eq. (5), $0 < z^* < z_{\rm cut}$ defines the separation between the center ($|z| < z^*$) and the edge ($z^* < |z| < z_{\rm cut}$) angular regions and is *a priori* arbitrary to some extent. In previous applications (see, for example, Refs. [13–17]), the "optimal" numerical value turned out to be $z^* \simeq 0.5$, and we shall keep this value of z^* here as well. One can notice that, by definition, $A_{\rm CE}$ is symmetric under $z \leftrightarrow -z$; hence it is insensitive to the sign of z. Moreover, being a ratio of integrated cross sections, an advantage of $A_{\rm CE}$ is that it should be less sensitive to theoretical systematic uncertainties, such as the uncertainties from different sets of parton distributions and from the particular choice of factorization and renormalization scales.

III. GRAVITON RESONANCE AND SCALAR EXCHANGES

We sketch here the models we are interested in, together with their features relevant to the resonance spin and the distinctive angular distributions for process (1).

A. RS model of gravity with one compactified extra dimension

This model, originally proposed as a solution to the gauge hierarchy problem $M_{\rm EW} \ll M_{\rm Pl}$, consists of two 3-branes, and one compactified warped extra spatial dimension y with exponential warp factor $\exp(-k\pi|y|)$ [1]. Here, $k > 0$ is the 5D curvature, assumed to be of the order of $M_{\rm Pl}$. The two branes are placed at orbifold fixed points, $y = 0$ with positive tension called the Planck brane, and the second brane at $y = R_c$ with negative tension called the TeV brane. The basic, simplifying hypothesis is that the SM fields are localized on the TeV brane, whereas gravity originates on the Planck brane but is allowed to propagate everywhere in the 5D space. The consequence of this setup is the existence of KK modes of the graviton that can be exchanged in the interactions among SM particles in the TeV brane. Owing to the exponentially suppressing warp factor, mass scales, in passing from the Planck brane to the TeV brane, can become the size of the TeV order. Moreover, a specific mass spectrum of such KK resonances is predicted in terms of an effective mass scale defined as $\Lambda_\pi = \bar{M}_{\rm Pl}\exp(-k\pi R_c)$, which for $kR_c \simeq 12$ happens to be of the TeV order (here $\bar{M}_{\rm Pl} = 1/\sqrt{8\pi G_{\rm N}}$, with $G_{\rm N}$ the Newton constant). These resonances, represented by spin-2 fields $h^{(n)}_{\mu\nu}$, can in process (1) show up as (narrow) peaks in $M_{\gamma\gamma} \equiv M$, through the interaction

$$\mathcal{L} = -\frac{1}{\Lambda_\pi} T^{\mu\nu} \sum_{n=1}^{\infty} h^{(n)}_{\mu\nu}. \tag{6}$$

Here $T^{\mu\nu}$ is the energy-momentum tensor of the SM; the characteristic mass spectrum is $M_n = x_n k \exp(-k\pi R_c)$ [with x_n the roots of the Bessel function $J_1(x_n) = 0$], and the resonance widths are $\Gamma_n = \rho M_n x_n^2 (k/\bar{M}_{\rm Pl})^2$, with ρ a calculable constant depending on the number of open decay channels, of the order of 0.1.

The model can therefore conveniently be parametrized in terms of $M_G \equiv M_1$, the mass of the lowest graviton excitation, and of the "universal" dimensionless graviton coupling $c = k/\bar{M}_{\rm Pl}$. Theoretically, the expected "natural" ranges for these parameters, avoiding additional mass hierarchies, are $0.01 < c < 0.1$ and $\Lambda_\pi < 10$ TeV [2]. The 95% CL experimental lower bounds on M_G from previous analyses vary, essentially, from 0.6 to 1.0 TeV as c ranges from 0.01 to 0.1 [5,6,26]. Quite recently, preliminary results from RS graviton searches in dilepton inclusive production at the 7 TeV LHC with luminosity 1.2 fb^{-1} indicate 95% CL lower limits on M_G of 0.7 TeV for $c = 0.01$ and up to 1.6–1.7 TeV for $c = 0.1$ [27,28].

In hadronic collisions, in QCD at LO, photon pairs can be produced via the quark-antiquark annihilation $q + \bar{q} \to \gamma + \gamma$ and the gluon-gluon fusion $g + g \to \gamma + \gamma$. The relevant diagrams at this order, for the SM and the RS graviton exchange, are represented in Figs. 1 and 2. Actually, the SM box diagram in Fig. 2 is of higher order in α_s and, as discussed in the next section, for the values of the $\gamma\gamma$ invariant

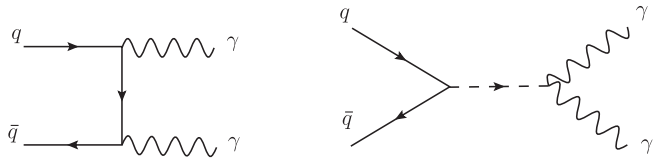

FIG. 1. Feynman diagrams contributing to the subprocess $q\bar{q} \to \gamma\gamma$, where the dashed line represents either a RS graviton KK mode G or a scalar exchange S. The crossed diagrams are not displayed.

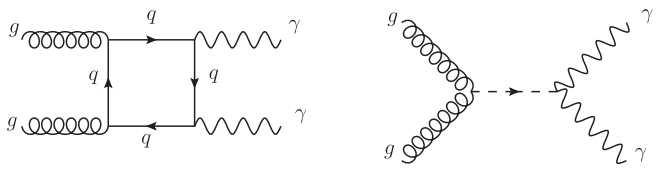

FIG. 2. Feynman diagrams contributing to the subprocess $gg \to \gamma\gamma$, including the exchange of either a RS graviton KK mode G or a scalar S which is denoted by the dashed line. The crossed diagrams are not displayed.

mass M in the TeV range of interest here, its contribution turns out to be negligible, as earlier noticed also in Ref. [29].

Using Feynman rules for graviton exchange [20,30], the z-even angular dependencies needed in (5) can be written as [31–33]

$$\frac{d\sigma(q\bar{q}\to\gamma\gamma)}{dz} = \frac{1}{192\pi\hat{s}}\Big[64\alpha^2\pi^2Q_q^4\frac{1+z^2}{1-z^2} + \frac{\hat{s}^4}{16}|C(\hat{s})|^2(1-z^4) - 4\pi\alpha Q_q^2\hat{s}^2\,\mathrm{Re}[C(\hat{s})](1+z^2)\Big], \quad (7)$$

where the subprocess Mandelstam variable is the diphoton invariant mass, $\sqrt{\hat{s}}\equiv M$, and α is the electromagnetic coupling constant, with Q_q the quark electric charge. Moreover, in Eq. (7), $C(\hat{s})$ represents the sum of KK graviton propagators with masses $M = M_n$ and widths Γ_n:

$$C(\hat{s}) = \frac{1}{\Lambda_\pi^2}\sum_n \frac{1}{\hat{s}-M_n^2+iM_n\Gamma_n}. \quad (8)$$

In practice, from the phenomenology, just the lowest graviton mass $M_G\equiv M_1$, and perhaps the next one, M_2, at most, can be expected to fall within the discovery reach of the LHC.

The cross section for the $gg\to\gamma\gamma$ subprocess via the RS graviton excitation exchange is

$$\frac{d\sigma(gg\to\gamma\gamma)}{dz} = \frac{\hat{s}^3}{8192\pi}|C(\hat{s})|^2(1+6z^2+z^4). \quad (9)$$

Notice that a factor $1/2$ is embodied in Eqs. (7) and (9) to account for the identical final state photons.

B. The model for scalar exchange

In principle, in order to discriminate the graviton spin-2 angular distribution from the spin-0 hypothesis, we might limit ourselves to make a comparison of Eqs. (7) and (9) with the results of a generic flat (in z) distribution numerically tuned to the same number of events around M_G. However, for the graviton exchange we shall use a description supplemented by the cross sections calculated to NLO in QCD and, to consistently fully exploit the QCD dynamics also for the spin-0 scenario, we need an explicit model for a scalar particle exchange with definite couplings to the SM fields, in particular, to photon pairs.

We consider the simple model of a scalar particle S singlet under the SM gauge group and with mass $M\equiv M_S$ of the TeV order, proposed in Ref. [23]. The trilinear couplings of S with gluons, electroweak gauge bosons, and fermions are in this model:

$$\mathcal{L} = c_3\frac{g_s^2}{\Lambda}G^a_{\mu\nu}G^{a\,\mu\nu}S + c_2\frac{g^2}{\Lambda}W^i_{\mu\nu}W^{i\,\mu\nu}S + c_1\frac{g'^2}{\Lambda}B_{\mu\nu}B^{\mu\nu}S + \sum_f c_f\frac{m_f}{\Lambda}\bar{f}fS. \quad (10)$$

In Eq. (10), Λ is a high mass scale, of the TeV order of magnitude, and c's are dimensionless coefficients that are assumed to be of order unity, reminiscent of a strong novel interaction. In our subsequent analysis we take, following Ref. [23], $\Lambda = 3$ TeV. As for the c's, we shall leave their numerical values free to vary in a range of the order of (or less than) unity, but constrained so that the scalar particle width Γ_S could be comparable to (or included in) the diphoton mass window ΔM of Eq. (4).

The leading order diphoton production process is in this model dominated by the s-channel exchange $gg\to S\to\gamma\gamma$. As it is of order α_s^2 at LO, it will be sensitive to the choice of this coupling constant. The Feynman diagrams in the scalar model will be similar to those in the RS model, as shown in Figs. 1 and 2 with the KK mode replaced by the scalar. The corresponding differential cross section reads, including a factor $1/2$ for identical final particles,

$$\frac{d\sigma(gg\to\gamma\gamma)}{dz} = \frac{1}{2}\frac{1}{16\pi}\left(\frac{c_3g_s^2}{\Lambda}\right)^2\left(\frac{(c_1+c_2)e^2}{\Lambda}\right)^2\hat{s}^3|D(\hat{s})|^2. \quad (11)$$

In Eq. (11), $D(\hat{s})$ is the scalar propagator,

$$D(\hat{s}) = \frac{1}{\hat{s}-M_S^2+iM_S\Gamma_S}, \quad (12)$$

and the expression of the total width Γ_S in terms of the c's and Λ introduced in Eq. (10) can be obtained from [23], by summing the partial widths reported there into gg (dominant, as is the cross section, proportional to c_3), $\gamma\gamma$, W^+W^-, ZZ, and $\bar{f}f$.

In Fig. 3 we represent, as an example, the domains in c_3 vs all other parameters c_i ($i\neq 3$) assumed equal to each other, allowed by the constraint $\Gamma_S\leq\Delta M$ for different values of M_S.

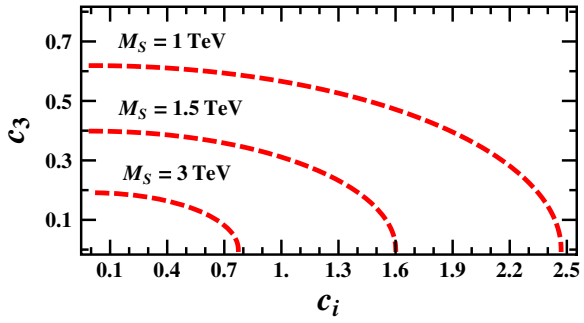

FIG. 3 (color online). The lines in the parameter plane (c_i, c_3) with equal c_i ($i\neq 3$) correspond to the solutions of the equation $\Gamma_S = \Delta M$ for $M_S = 1$ TeV, 1.5 TeV and 3 TeV, $\Lambda = 3$ TeV. The allowed area is at the left of these lines.

As the coupling of the scalar particle to quarks is proportional to the quark mass much smaller than Λ, one can neglect at LO the subprocess $\bar{q}q \to S \to \gamma\gamma$, and the cross section for $pp \to S \to \gamma\gamma$ will be expressed simply by the gluon-initiated process plus the SM contribution appearing in Eq. (7). Thus, at this LO, there is, in the considered spin-0 model, no interference between the SM quark-initiated contribution and the scalar-exchange amplitude. However, quark contributions cannot be neglected at the NLO QCD order and, in particular, a (small) interference of the gg SM box diagram with the gg scalar exchange will occur, as will be specified in the next section.

Preliminary to the numerical analysis of $A_{\rm CE}$, in the next section we briefly describe the estimate of the next-to-leading order QCD effects.

IV. NEXT-TO-LEADING ORDER QCD EFFECTS

A. Outline of the calculational procedure

The diphotons produced in hadronic collisions could originate from the hard partonic interaction (direct photon), or at least one photon could be produced in the hadronization of a parton (fragmentation photon). Of course, our aim here is to emphasize the sensitivity to diphotons produced by the RS resonance exchange (the signal). In the experimental analysis, hadronic jets can, in principle, mimic isolated photons. Such backgrounds, mainly originating from dijet production and prompt photon plus jet production, can be measured at "low" diphoton invariant mass, of the order of few hundreds of GeV, and extrapolated to higher invariant mass. At invariant mass scales in the TeV range of interest here, the SM diphoton production seems to largely dominate the background; see, for example, Ref. [34].

In our calculation, in addition to the cuts relevant to the ATLAS experiment listed in Sec. II, we implement photons isolation by defining "cones" in the rapidity-azimuthal plane (η, ϕ):

$$R(i,j) = \sqrt{(\eta_i - \eta_j)^2 + (\phi_i - \phi_j)^2}, \qquad (13)$$

and imposing the criterion that events with $R < R_0$ should be discarded. Specifically, two-photon events should be discarded if $R(\gamma, \gamma) < R_0$, and we take the "conventional" value $R_0 = 0.4$. Moreover, at NLO, one expects soft and collinear singularities of QCD as well as of QED origin, related to massless partons. In particular, collinear QED singularities originating from emission of a final state photon from a quark or an antiquark could, in principle, be eliminated by factoring them out and absorbing them into parton fragmentation functions. However, the fragmentation functions are additional nonperturbative inputs that are not well understood. Therefore, as an alternate approach to isolate direct photons from hadronic jets, we use the so-called smooth cone isolation prescription of Ref. [35], which ensures that the fragmentation contributions are suppressed without affecting the cancellation of the conventional QCD singularities, so that infrared safe cuts can be applied. Basically, the prescription consists in discarding the events for which the cone $R(\gamma, \text{jet}) < R_0$; we assume $R_0 = 0.4$ again, and the associated hadronic transverse energy is $E_T^{\rm had} > E_{T\,\rm max}$. One can parametrize $E_{T\,\rm max}$ as $E_{T\,\rm max} = E_T^{\rm iso}\{(1 - \cos R)/(1 - \cos R_0)\}^n$, and we take the values $E_T^{\rm iso} = 15$ GeV and $n = 2$ (numerically, the dependence on n turns out to be negligible).

We now start from the extra dimension scenario, where the NLO corrections in QCD were considered for a phenomenologically interesting process like the dilepton [36–38] and diphoton production [39,40] at hadron colliders. The essential Feynman rules for KK modes coupling to ghosts and a KK mode propagator in $(4 + \epsilon)$ dimensions needed for the NLO computation have been introduced in [36]. For the diphoton computation a semi-analytical two-cutoff phase space slicing method [41] to deal with various singularities of IR and collinear origin that appear at NLO in QCD was used. After cancellation and mass factorization of these singularities, the remaining finite part is numerically integrated over the phase space by using Monte Carlo techniques.

As stated in previous sections, diphotons can, in the SM, be produced to LO in QCD, in the quark-antiquark annihilation subprocess $q\bar{q} \to \gamma\gamma$. Photon pairs produced via the gluon fusion subprocess through a quark box diagram $gg \to \gamma\gamma$, though of the order α_s^2, have cross sections comparable to those of the $q\bar{q} \to \gamma\gamma$ subprocess for the low diphoton invariant mass. In the light Higgs boson searches, this subprocess plays an important role, due to the large gluon flux at small fractional momentum x, and is formally treated as a LO contribution, although it is of $\mathcal{O}(\alpha_s^2)$, and hence is, in reality, a next-to-next-to-leading order contribution. However, it falls off rapidly with increasing diphoton invariant mass, and in the mass range of interest for the TeV scale gravity models, it need not be included at LO. It has been demonstrated in [39,40] that the contribution of this subprocess in the SM is a few orders of magnitude smaller than that of the $q\bar{q}$ subprocess for diphoton invariant mass $M > 500$ GeV.[1]

The NLO QCD corrections to the diphoton production process would involve real emission diagrams corresponding to the following $2 \to 3$ subprocesses: (a) $q\bar{q} \to \gamma\gamma g$ (Fig. 4), (b) $gg \to \gamma\gamma g$ (Fig. 5), and (c) $gq(\bar{q}) \to \gamma\gamma q(\bar{q})$ (the gq diagrams can be obtained from the $q\bar{q}$ diagram by an appropriate interchange of initial and final state particles). In the virtual part, $\mathcal{O}(\alpha_s)$ corrections at one loop arise as a result of the interference between the one-loop graphs at $\mathcal{O}(\alpha_s)$ of (SM + NP) and the Born graphs at $\mathcal{O}(\alpha_s^0)$ of (SM + NP). Some of the typical NP one-loop Feynman diagrams to $\mathcal{O}(\alpha_s)$ are shown in Fig. 6. The $q\bar{q}$ channel gets such contributions from both the SM and the graviton

[1] See also the discussion of the SM NLO predictions for process (1) in Ref. [42].

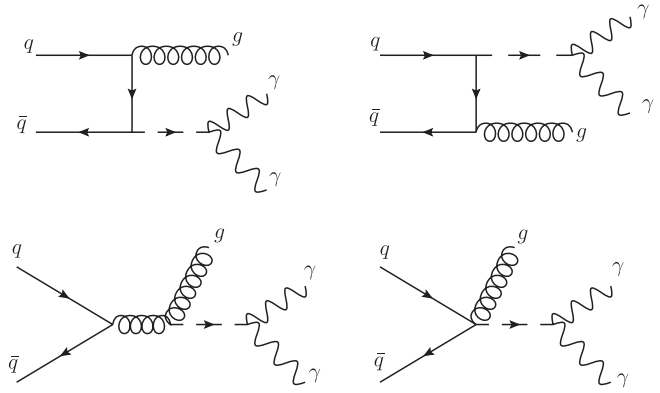

FIG. 4. Feynman diagrams contributing to the subprocess $q\bar{q} \to \gamma\gamma g$. The dashed line could be either $R = G$ or S depending on the model. For the scalar exchange S the last diagram involving a four-point vertex does not exist.

exchange, while in the gg channel the SM contribution already begins at $\mathcal{O}(\alpha_s)$. The SM $gg \to \gamma\gamma$ subprocess amplitude can interfere with the gluon-initiated LO gravity exchange subprocess, giving a $\mathcal{O}(\alpha_s)$ contribution, Fig. 2. In the qg channel there is no virtual contribution to this order in either the SM or the NP models of interest here.

Both the virtual and real corrections have been evaluated with five quark flavors and in the limit of vanishing quark masses. The n-point tensor integrals appearing from integration over loop momenta were simplified using the Passarino-Veltman reduction [43]; the computation was done using dimensional regularization in $(4 + \epsilon)$ dimensions, in the $\overline{\text{MS}}$ scheme.

The virtual contribution here does not contain UV singularities; this can be attributed to the facts that (i) the electromagnetic current is conserved and does not receive any

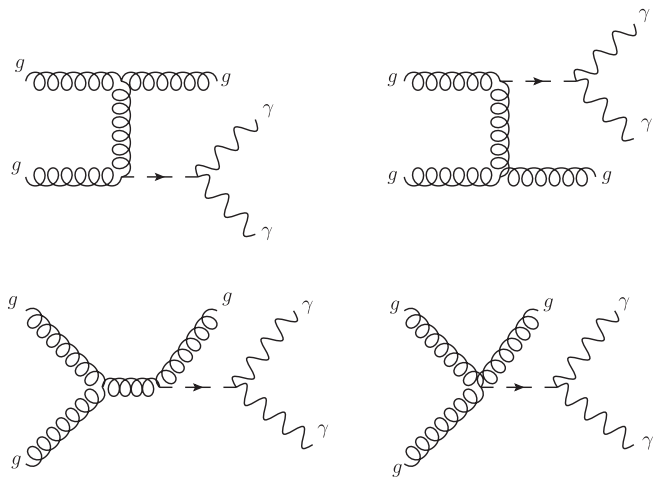

FIG. 5. Feynman diagrams contributing to the subprocess $gg \to \gamma\gamma g$, where the dashed line corresponds to a spin-2 RS KK mode G or a scalar exchange S. In the case of a scalar exchange the last diagram involving a four-point vertex does not exist.

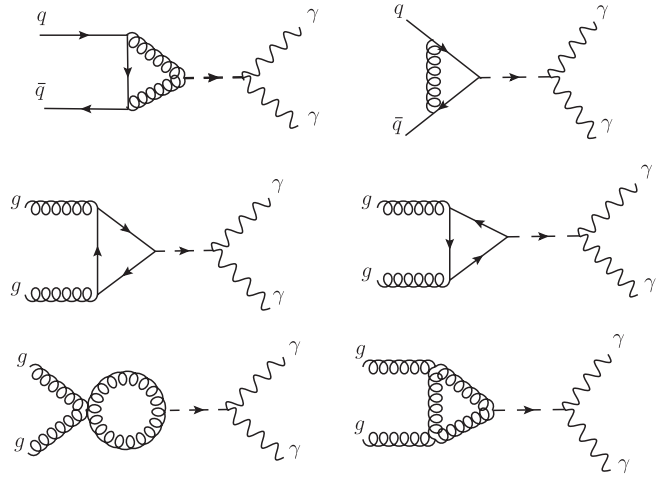

FIG. 6. Feynman diagrams contributing to a one-loop subprocess to the $q\bar{q}$ and gg channels in the NP models.

QCD corrections, and (ii) the graviton couples to the energy-momentum tensor of the SM fields which is a conserved quantity and therefore is not renormalized. The poles in ϵ arise from loop integrals and correspond to the soft and collinear divergences; configurations where a virtual gluon momentum goes to zero give soft singularities, while the collinear singularities arise when two massless partons become collinear to each other.

The three-body phase space of the real emission diagrams has regions which are soft and collinear divergent. The phase space can accordingly be separated into soft (s) and hard regions and, furthermore, the hard region can be separated into hard collinear (HC) and hard noncollinear ($\overline{\text{HC}}$) parts as follows:

$$d\sigma^{\text{real}} = d\sigma_s^{\text{real}}(\delta_s) + d\sigma_{\text{HC}}^{\text{real}}(\delta_s, \delta_c) + d\sigma_{\overline{\text{HC}}}^{\text{real}}(\delta_s, \delta_c). \quad (14)$$

The small cutoff parameters δ_s and δ_c set arbitrary boundaries for the soft (gluon energy $0 \le E_g \le \delta_s\sqrt{\hat{s}}/2$) and collinear ($0 \le \hat{t}_{ij} \le \delta_c\hat{s}$) regions, respectively. Here, for the $2 \to 3$ process with momenta $p_1 + p_2 = p_3 + p_4 + p_5$, the Mandelstam variables are defined as $\hat{s}_{ij} = (p_i + p_j)^2$, $\hat{t}_{ij} = (p_i - p_j)^2$, with $\hat{s} = \hat{s}_{12}$. In these mutually exclusive soft and hard collinear regions, the three-body cross section can be factored into the Born, $2 \to 2$, cross section and the remaining phase space integral can easily be evaluated in $(4 + \epsilon)$ dimensions to get the expansion of the soft and collinear singularities in powers of ϵ. All positive powers of the small cutoff parameters δ_s and δ_c are set to zero; only logarithms of the cutoff parameters are retained. Adding the virtual and real contributions, all double and single poles of IR origin are automatically canceled between the virtual and the first two terms of Eq. (14). The remaining collinear poles are absorbed into the parton distribution functions.

The hard noncollinear part in Eq. (14) corresponds to the three-body phase space, which by construction is finite, and can be evaluated in four dimensions ($\epsilon = 0$). The sum of real and virtual contributions is now free of singularities and can hence be evaluated numerically by using a Monte Carlo method. It can be further seen that the explicit logarithmic dependence on δ_s and δ_c in the two-body phase space $[d\sigma_s^{\rm real}(\delta_s) + d\sigma_{\rm HC}^{\rm real}(\delta_s, \delta_c)]$ is canceled by the implicit dependence of the three-body hard noncollinear part $d\sigma_{\rm HC}^{\rm real}(\delta_s, \delta_c)$ on these parameters, after the numerical integration is carried out. The sum of the two-body and three-body parts in Eq. (14) would be independent of the slicing parameters δ_s and δ_c, which is explicitly verified before the code is used for the analysis. Now these codes [39,40] can be used to study the full quantitative implication of the NLO QCD corrections to the various distributions of interest in the extra dimension searches.

Turning to the scalar-exchange model, the matrix elements corresponding to the interference between the SM box diagram and the LO gg-initiated tree-level diagram are given by

$$I^{gg}_{\rm SM*S}(z) = \frac{g_s^2}{16\pi^2} Q_q^2 \,{\rm Re}[D(\hat{s})] \frac{1}{[N^2-1]} \left(\frac{c_3 g_s^2}{\Lambda}\right) \times \left(\frac{(c_1+c_2)e^2}{\Lambda}\right) \left\{ \left(\frac{\hat{t}-\hat{u}}{2}\right) \left[\ln\left(\frac{-\hat{t}}{\hat{s}}\right) - \ln\left(\frac{-\hat{u}}{\hat{s}}\right) \right] - \left(\frac{\hat{u}^2+\hat{t}^2}{2\hat{s}}\right) \left[{\rm Li}_2\left(\frac{-\hat{u}}{\hat{t}}\right) + {\rm Li}_2\left(\frac{-\hat{t}}{\hat{u}}\right) - 2\zeta(2) \right] \right\}, \tag{15}$$

where $\hat{s}$, $\hat{t} = -\frac{\hat{s}}{2}(1-z)$, $\hat{u} = -\frac{\hat{s}}{2}(1+z)$ are the usual Mandelstam variables, N are the color degrees of freedom, and $\zeta(2) = \pi^2/6$ is the Riemann zeta function.

In the scalar model, the UV divergences in the virtual corrections to the gg-initiated diphoton production process are removed by renormalization. The remaining finite contribution is given by

$$\frac{d\sigma_v}{dz} = \frac{g_s^2}{16\pi^2} 8N\zeta(2) \frac{d\sigma}{dz}, \tag{16}$$

where $d\sigma/dz$ is the Born contribution given in Eq. (11). The remaining soft and collinear finite contributions

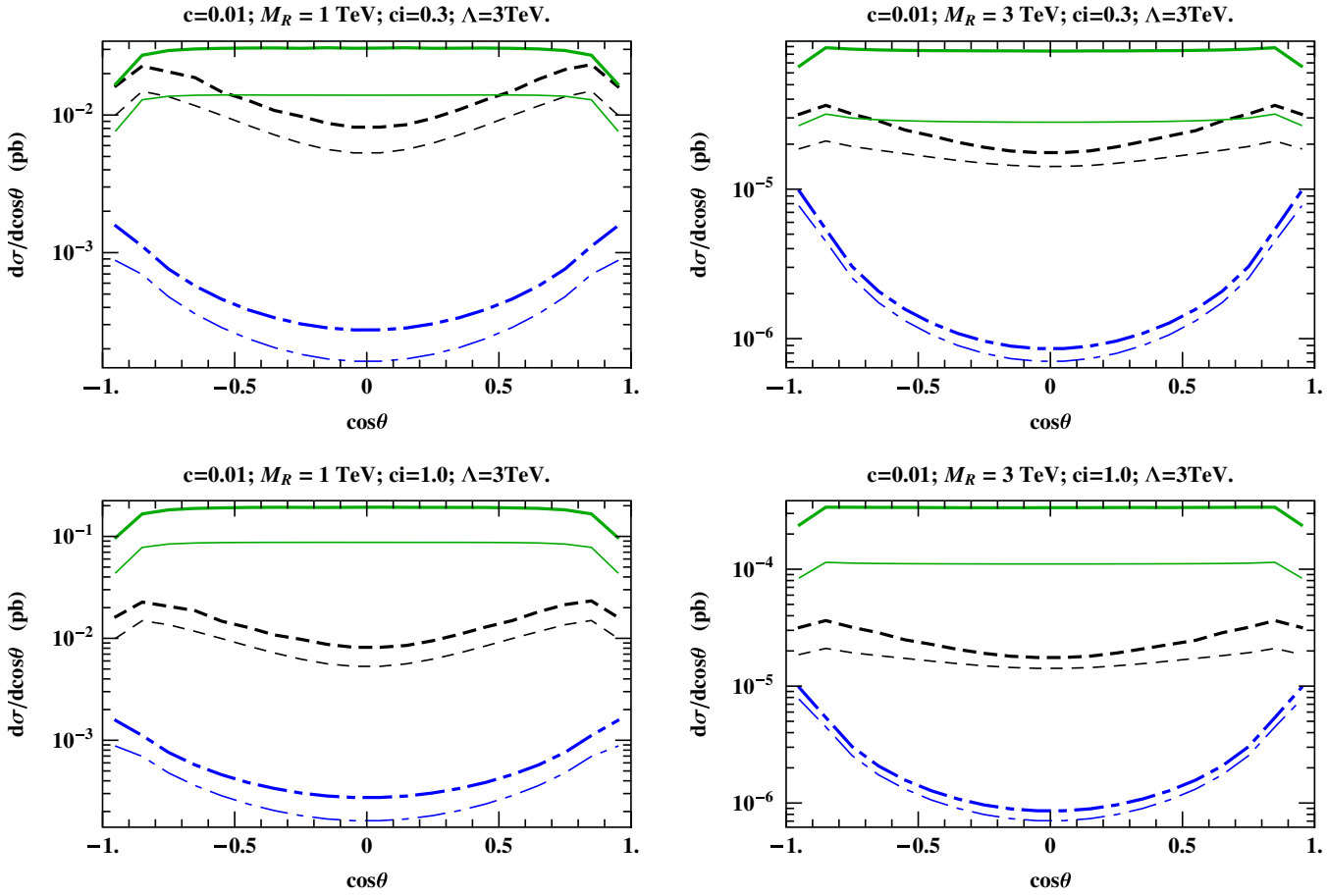

FIG. 7 (color online). Angular distributions of photons for the process $p + p \to \gamma\gamma + X$ with $M_R = 1$ TeV and 3 TeV at the 14 TeV LHC in the SM (dot-dashed blue lines), the RS model with graviton coupling constant $c = 0.01$ (black dashed lines), and the scalar resonance model (green solid lines) with $c_3 = 0.3$, $c_i = 0.3$, $i \neq 3$ (left and right top panels) and $c_3 = 0.3$, $c_i = 1.0$ (left and right bottom panels). Thin and thick lines represent the LO and the NLO calculations, respectively.

coming from the real corrections to the LO scalar model diagram are proportional to the Born cross section. As they originate from pure QCD, they are independent of the hard scattering process; hence they will be the same as those for the s-channel diphoton production process in the RS model and are given in Ref. [39].

At the NLO in QCD, the following three subprocesses contribute to the scalar model cross section: (i) $\bar{q}q \to gS$, (ii) $qg \to qS$, and (iii) $gg \to gS$, all followed by $S \to \gamma\gamma$. The Feynman diagrams for the $\bar{q}q$ and gg channels are given in Figs. 4 and 5, respectively, wherein the dashed line now represents the scalar S and the four-point diagrams will be absent for the scalar case. The couplings of S to the light quarks are proportional to the masses and hence are negligible so that the main contribution to the $\bar{q}q$ channel is from the S coupling to the gluons. Again the qg channel is related to the $\bar{q}q$ channel by a suitable change of initial and final states.

B. Numerical results for NLO corrections

Figure 7 shows, as an example, for the diphoton resonance mass values $M_R = 1$ and 3 TeV, the angular distributions at the 14 TeV LHC, at LO and NLO, for the cases of the SM, the SM plus the RS graviton exchange with

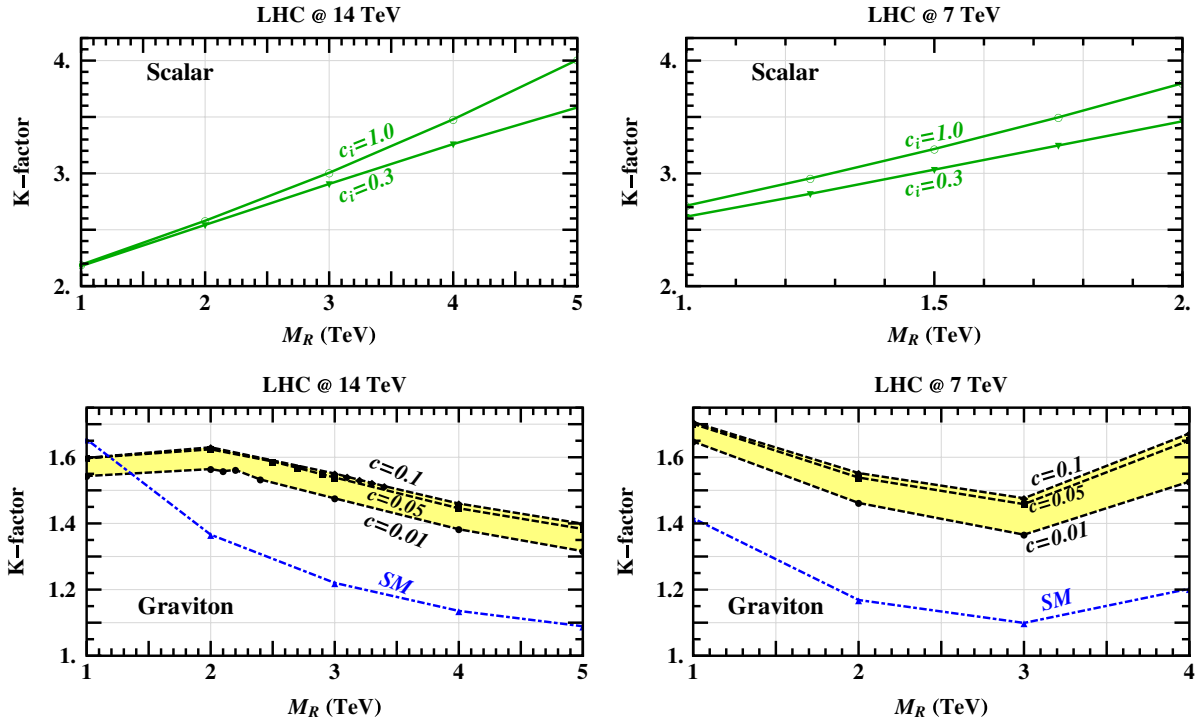

FIG. 8 (color online). K-factor vs M_R for the 14 TeV (left panel) and 7 TeV (right panel) LHC.

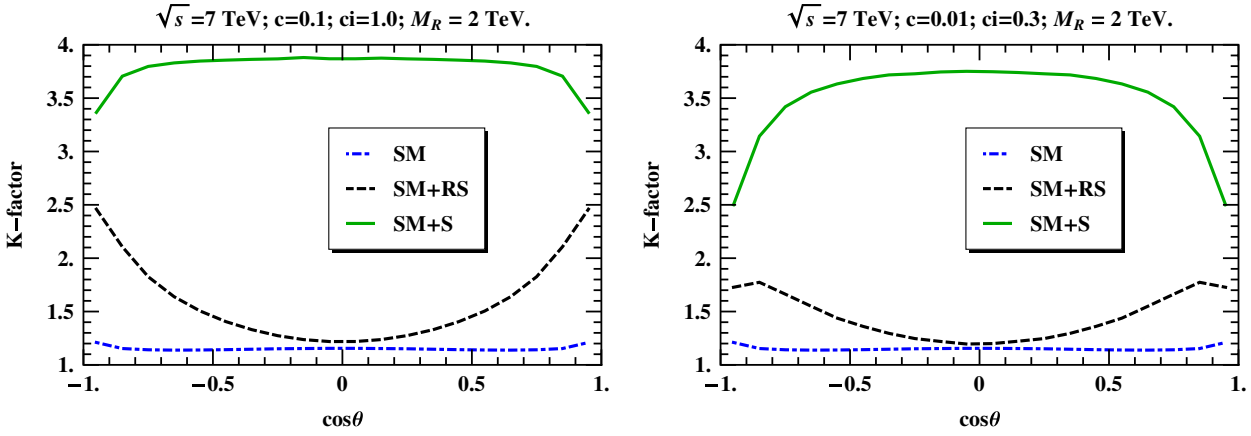

FIG. 9 (color online). K-factor vs cosθ for the 7 TeV LHC.

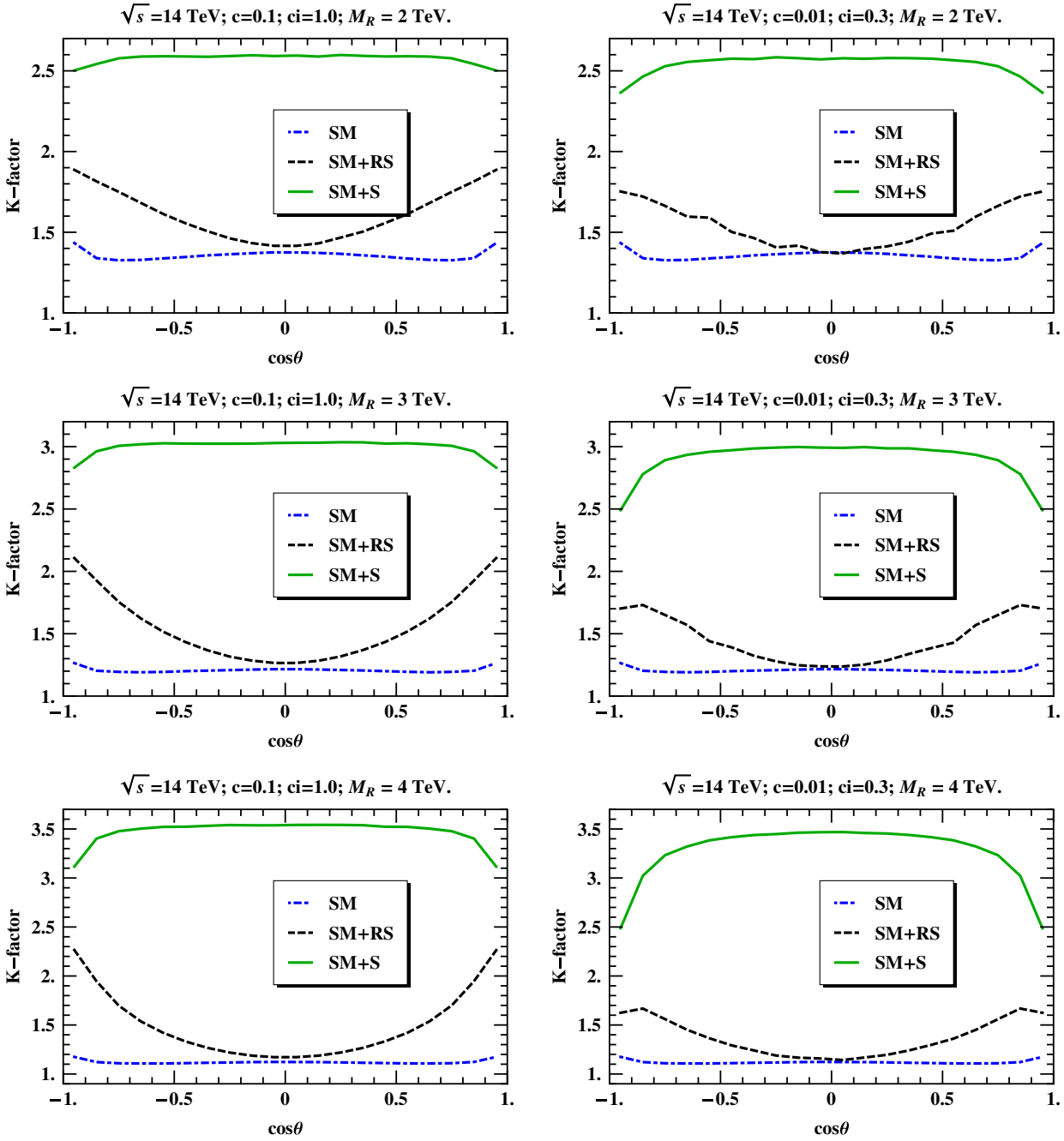

FIG. 10 (color online). K-factor vs cosθ for the 14 TeV LHC.

coupling constant $c = 0.01$, and the SM plus scalar particle exchange with couplings $(c_3 = c_i = 0.3)$ and $(c_3 = 0.3, c_i = 1.0)$, $i \neq 3$.

K-factors represent, quantitatively, the magnitude of the NLO QCD corrections, and are defined as the ratio of the NLO cross section to the corresponding LO one as follows:

$$\mathrm{K} = \frac{\sigma_{\mathrm{SM}}^{\mathrm{NLO}} + \sigma_{\mathrm{NP}}^{\mathrm{NLO}}}{\sigma_{\mathrm{SM}}^{\mathrm{LO}} + \sigma_{\mathrm{NP}}^{\mathrm{LO}}}. \tag{17}$$

Here, the subscript "NP" refers to the new physics contribution (extra dimension or scalar exchange) and its interference with the SM to LO or NLO as the case may be, while the subscript "SM" refers to only the SM contribution. The ratio could be of total cross sections, as is the case of Fig. 8, or of angular distributions, as is the case of Figs. 9 and 10. Including higher order QCD corrections to an observable at the hadron collider reduces the dependence on the factorization and renormalization scales; furthermore, since the K-factor itself could be large, it is essential to include these corrections.

The dependence of the K-factors on the coupling constant c in the RS case, exhibited in the lower panel of

Fig. 8, can be understood by the fact that, for low values of $c \sim 0.01$, the NP interference with the SM could be of the same order as the pure NP part. For values of $c > 0.05$, the SM contribution is negligibly smaller than the pure NP part and can be neglected both in the numerator and in the denominator of Eq. (17), which in this case is determined by the NP solely so that the dependence from c cancels. It is interesting to notice from the upper panel of Fig. 8 that the K-factors in the scalar case are larger than those in the RS case: the NLO corrections have enhanced the cross sections but, as shown in Figs. 9 and 10, they did not noticeably change the shape of the angular distributions from the flat behavior of the pure scalar particle exchange cross section in Eq. (11).

Also, one may remark that in the example discussed here the RS graviton couples to quarks and gluons with equal coupling strength whereas, in the model of Ref. [23] we have adopted, the scalar particle couples mainly to gluons (couplings to quarks are identically zero in the limit of vanishing quark masses). Furthermore, the production of a scalar particle in the gluon-gluon fusion subprocess is *qualitatively* equivalent to the Higgs boson production in the limit of infinite top quark mass: it is well known that K-factors (due to NLO QCD corrections) for the Higgs production process at hadron colliders are very high and can easily be greater than 2.0 in the light Higgs mass region [44–46]. Hence, a similar pattern of K-factors can be expected in the case of scalar production (followed by decay to photons) in the model considered here; see Figs. 8–10.

V. ANGULAR ANALYSIS AND RS GRAVITON IDENTIFICATION

The $A_{\rm CE}$-based angular analysis will essentially proceed as follows. The first step will be the determination of graviton-scalar ''confusion regions,'' namely, of the subdomains in respective discovery signature spaces of coupling constants and masses where, for $M_R = M_G = M_S$, the two models predict equal numbers of resonance signal events, N_S, and hence are not directly distinguishable on a statistical basis. In such confusion regions, one can then try to discriminate the models from one another by means of the different values of the $A_{\rm CE}$ asymmetry generated by the respective photon angular distributions.

After having presented the K-factors in Figs. 8–10, in Fig. 11 we show as an example the representation of $A_{\rm CE}$ vs z^* predicted at the 14 TeV LHC at LO and NLO for the two models we want to compare, with diphoton resonance invariant masses of 2 and 4 TeV. In this figure, the dashed and dot-dashed lines represent $A_{\rm CE}$ for the spin-2 case at NLO and LO, respectively, and the long-dashed and solid lines are the analogous ones for the spin-0 case. As one can see, an important feature of the NLO corrections is that, for the scalar exchange, $A_{\rm CE}$ is practically unaffected, the K-factor remaining almost flat in $\cos\theta$, whereas this is not so for the spin-2 case: the NLO effects tend to enlarge the difference between the $A_{\rm CE}$ relevant to the two cases, indicating a better possibility of distinguishing the models by the measurement of this observable.

Moreover, previous studies in Refs. [36–40], have shown the role of NLO corrections in substantially reducing the scale uncertainties on cross sections present in the LO results. This must be even more true for the ratio $A_{\rm CE}$ of Eq. (5), where both the numerator and the denominator have been predicted by a full NLO calculation. Further following [34], we expect that the sensitivity of this observable to the choice of parton distribution functions will be minimal.[2]

Thus, one can start from the assumption that an observed peak at $M = M_R$ is due to the lightest spin-2 RS graviton (thus, that $M_R = M_G$), and define a ''distance'' from the scalar-exchange model hypothesis as

$$\Delta A^G_{\rm CE} = A^G_{\rm CE} - A^S_{\rm CE}. \tag{18}$$

An indication of the domain in the (M_G, c) RS parameter plane, where the competing spin-0 hypothesis giving the same number of resonant events for $M_R = M_S = M_G$ can be excluded by the starting RS graviton hypothesis, can be obtained from a simpleminded χ^2-like numerical procedure, similar to that adopted in Ref. [13]. The comparison of the deviations (18) to the statistical uncertainty $\delta A^G_{\rm CE}$ pertinent to the RS model suggests the following criterion for spin-0 exclusion:

$$\chi^2 \equiv |\Delta A^G_{\rm CE}/\delta A^G_{\rm CE}|^2 > \chi^2_{\rm CL}. \tag{19}$$

Equation (19) shows the definition of the χ^2, and $\chi^2_{\rm CL}$ specifies a desired scalar-exchange exclusion confidence level (for example, $\chi^2_{\rm CL} = 3.84$ for 95% CL). With $\Delta A^G_{\rm CE}$ calculated in terms of M_R and of the model coupling constants, this condition will define the domain in the confusion regions of the model parameters where the RS spin-2 hypothesis can be discriminated from the scalar exchange. With $(A^G_{\rm CE})^2$ much smaller than unity for values of z^* around 0.5, we have a good approximation:

$$\delta A^G_{\rm CE} = \sqrt{\frac{1 - (A^G_{\rm CE})^2}{N_{S,\rm min}}} \approx \sqrt{\frac{1}{N_{S,\rm min}}}, \tag{20}$$

where $N_{S,\rm min}$ will be the minimum number of RS resonance events needed to satisfy the criterion (19), and hence to exclude the spin-0 exchange model with the same $M_R = M_G = M_S$ in the confusion region of the parameters. The knowledge of $N_{S,\rm min}$ determines, in turn, the RS resonance identification subdomain in the (M_G, c) parameter plane.

[2]Indeed, the uncertainties on the cross sections (at the percent level) used in simulations of experimental acceptances seem to support this point [34].

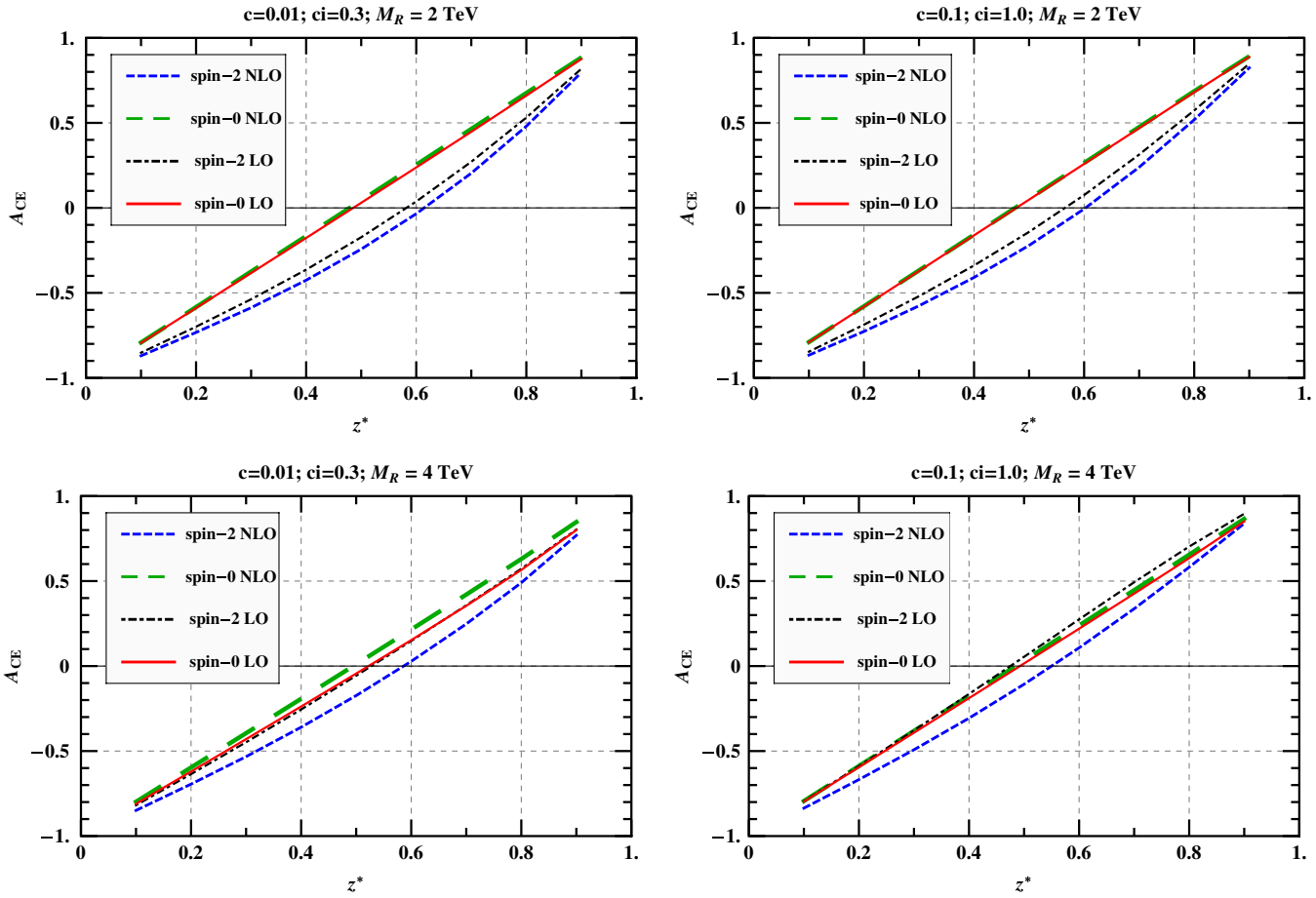

FIG. 11 (color online). LO and NLO A_{CE} asymmetry vs z^* for the inclusive process (1) at the 14 TeV LHC for the RS model with graviton coupling constant $c = 0.01(0.1)$, and the scalar resonance model with $c_3 = 0.3$, $c_i = 0.3$ ($c_3 = 0.3$, $c_i = 1.0$). Top-left panel (top-right panel): $M_R = 2$ TeV. Bottom panels: same as for top panels, but with $M_R = 4$ TeV.

We apply this procedure to the design LHC running conditions $\sqrt{s} = 14$ TeV and time-integrated luminosity $\mathcal{L}_{\text{int}} = 100$ fb^{-1}. Figure 12 shows the RS graviton signature domain for $0.01 \leq c \leq 0.1$ at LO (left panel) and to NLO (right panel) in QCD. The thick solid red line labeled "Discovery" indicates the minimum number of events statistically needed for the RS KK resonance discovery in process (1) at the 5σ level, as anticipated in Sec. II. The domain between the lines labeled by $c = 0.01$ and $c = 0.1$ represents the number of events for RS KK graviton production followed by decay into a photon pair, theoretically evaluated as described in the previous section, for different values of M_G. The scalar resonance signature space is also included in this figure, at the same LO and NLO, for simplicity, by the representative lines labeled $c_3 = c_i = 0.3$ and $c_3 = 0.3$, $c_i = 1.0$ ($i \neq 3$), respectively. One can see that, for these values of the scalar coupling constants, there is a finite confusion region where, at a given mass $M_R = M_G = M_S$, the numbers of predicted resonance signal events can be equal to each other. Actually, such a confusion region might easily be extended to almost completely overlap with the full RS signature space by partially weakening the condition $\Gamma_S \leq \Delta M$. This condition is, anyway, to be understood in a qualitative sense, so that more numerical freedom to the scalar coupling constants of Eq. (10) might be allowed. Indeed, if the width Γ_S turned out to be larger than ΔM in Eq. (4), the analysis proposed here should still be viable, and could in this case discriminate a narrow KK graviton vs the scalar resonances, both by the angular observable A_{CE} and by the size of the widths themselves. Also, we can remark that, as relying just on specific angular distributions, the kind of analysis proposed here should be applicable, more generally, to the identification of the RS graviton excitation from different scalar-exchange models than studied here.

The line labeled "ID" in Fig. 12 essentially represents the solution of Eq. (19) relating M_G to c; i.e., it is the minimum number of events needed for a discovered RS graviton resonance to be identified at 95% CL against the scalar particle exchange hypothesis, according to the A_{CE}-based angular analysis. The differences between the left and right panels clearly show the need to account for the large NLO QCD effects in the theoretical description of the resonant diphoton inclusive production at the LHC.

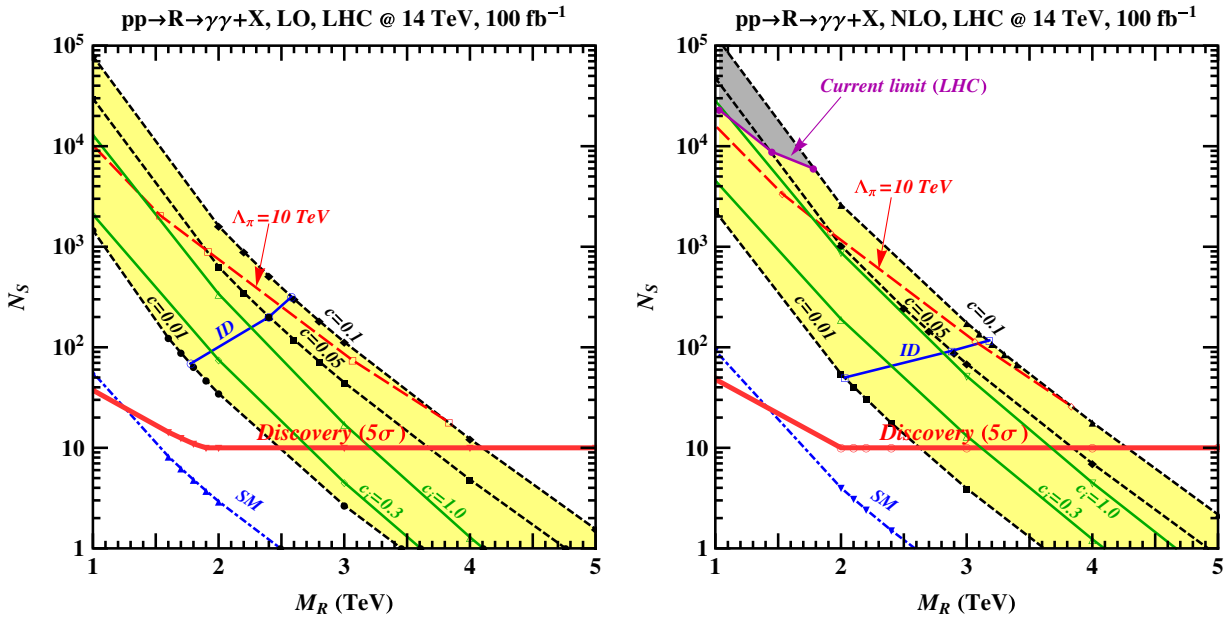

FIG. 12 (color online). Number of resonance (signal) events N_S vs M_R ($R = G$, S) at the LHC with $\sqrt{s} = 14$ TeV and $\mathcal{L}_{\rm int} = 100$ fb^{-1} for the process $pp \to G \to \gamma\gamma + X$ at LO (left panel) and NLO (right panel) QCD. The black dashed lines delimit the KK graviton signature space for $0.01 \le c \le 0.1$; the solid green lines represent the scalar S resonance signature as specified in the text; the thin solid red line shows current limits from the LHC; the long-dashed red line is for $\Lambda_\pi = 10$ TeV; the solid blue "ID" line shows $N_{S,\rm min}$ for the RS identification.

In practice, as one can read from the right, next-to-leading order panel in Fig. 12, if an RS graviton excitation is discovered in diphoton events at the 14 TeV LHC with 100 fb^{-1} luminosity, its spin may be identified for M_G up to, roughly, 2–3 TeV for $c = 0.01$–0.1 if the number of observed RS resonance signal events is larger than or equal to those indicated by the line "ID," namely, $N_{S,\rm min} \gtrsim 50$–120. Of course, these indications follow from the criterion (19) outlined above, and hence rely on statistical arguments and theoretical calculations of the relevant cross sections; in particular, one may notice in this regard that the SM background turns out to be completely negligible with respect to the signal. The detailed assessment of the "experimental" backgrounds to the resonance discovery in process (1), and of the related systematic uncertainties, is out of the scope of this paper; our purpose here is to just compare (and discriminate) two different theoretical explanations for the same resonance mass events, once observed, on the basis of NLO calculations in QCD.

The grey area in the right panel of Fig. 12 represents the 95% CL exclusion, where the RS resonance should not be observable, if we account for the lower limits on M_G vs c derived from the dilepton production analysis recently presented in Refs. [27,28]. Thus, the range in M_R of interest would start, in view of these LHC results, from $M_G =$ 1.6–1.7 TeV for $c = 0.1$ and $M_G = 0.7$ TeV for $c = 0.01$.

Also drawn in Fig. 12 is the line $\Lambda_\pi = 10$ TeV: the "theoretical" condition $\Lambda_\pi < 10$ TeV mentioned in Sec. III, if enforced literally, would dramatically constrain the RS discovery domain in the plane (M_G, c) to the events located above this line. However, this condition should also be understood in a qualitative sense, as is the case, in principle, of the assumed range of values for c.

To make contact with the current LHC running conditions, we repeat the RS identification procedure outlined above for the 7 TeV case, with time-integrated luminosities $\mathcal{L}_{\rm int} = 1$ and 10 fb^{-1}. The analogue of Fig. 12, but this time for the NLO calculations only, is represented in Fig. 13, with the same significance of the symbols. The interpretation of the left and right panels in this figure is also completely analogous. For example, if a RS resonance were discovered in diphoton events at 1 fb^{-1}, its spin-2 might be identified, to 95% CL, up to $M_G = 1.2$ TeV for $c = 0.1$, provided the collected signal was about 60 events; and for 10 fb^{-1}, identification would be possible up to $M_G = 1.5$ TeV for $c = 0.1$ with a collected signal of, say, about 100 events.

However, the situation is drastically modified by the 95% CL exclusion limits from the dilepton analysis of Refs. [27,28] at 1.2 fb^{-1}, reported in Sec. III and represented by the grey areas in both panels of Fig. 13. The experimental limit $M_G > 1.6$–1.7 TeV for $c = 0.1$ is not quite inconsistent with the left panel of Fig. 13, which shows that for these values the theoretically predicted statistics for RS events falls below that needed for 5σ discovery. The exclusion range starts from the low values $c = 0.01$ and $M_G = 0.7$ TeV, so that the left panel of this figure shows that, at the present stage, in principle, there may still be a little corner available for discovery, roughly M_G between 0.7 and 1.3 TeV and small $c < 0.05$. On the

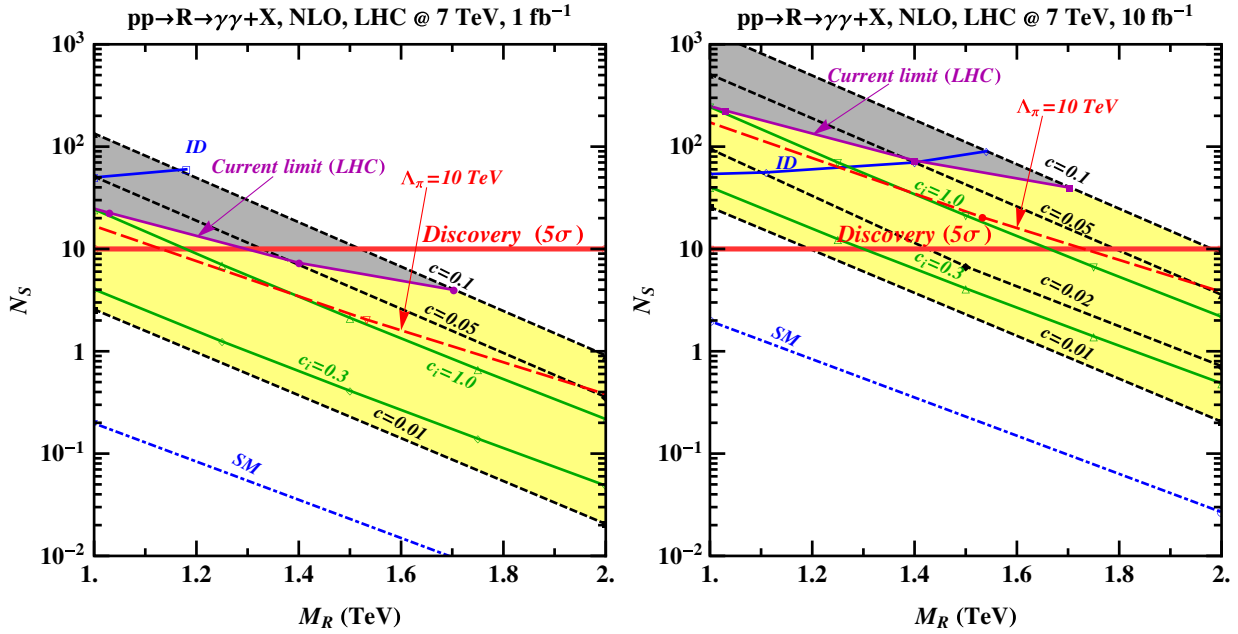

FIG. 13 (color online). Similar to Fig. 12, but for NLO QCD at $\sqrt{s} = 7$ TeV and $\mathcal{L}_{\rm int} = 1$ fb^{-1} (left panel) and $\mathcal{L}_{\rm int} = 10$ fb^{-1} (right panel).

other hand, this panel clearly indicates that there is no room for RS graviton identification at 1 fb^{-1} luminosity, at least with the angular analysis presented here. Moving to the 10 fb^{-1} case, the right panel of Fig. 13 shows that, with the current LHC limits, discovery might still be possible up to about $M_G = 2$ TeV with $c = 0.1$, but the identification would be allowed only for $M_G = 0.7$–1.4 TeV with c not larger than, say, 0.05.

VI. FINAL CONSIDERATIONS

In the previous sections, we have discussed the features of different-spin s-channel exchanges in the inclusive diphoton production process (1) at the LHC. Specifically, we have considered the hypothesis of the spin-2 RS graviton excitation exchange as the source of an eventually discovered peak in the diphoton invariant mass, and have compared it with the interpretation of the same peak as that of a spin-0 scalar exchange, exemplified by the model [23]. The aim has been to determine quantitatively the domain in the RS graviton mass M_G and coupling constant $c = k/\bar{M}_{\rm Pl}$, where the former hypothesis can be identified against the latter (the so-called identification reach).

Clearly, to this purpose, in the situation of an equal number of peak events from the two models, the information from the distinctive photon angular distributions is needed. The relevant cross sections, differential and angular integrated, at next-to-leading order in QCD have been introduced for both the RS and the scalar-exchange model. The comparison with the leading order calculations shows that the NLO effects are substantial, and non-negligible for this analysis. As shown in Sec. IV, in the TeV resonance mass range of interest here and at the considered LHC energies, K-factors turn out to be large, of the order of 1.5 or so for the RS exchange, and even larger, of the order of 3 or so, for the scalar-exchange model. Moreover, while K-factors exhibit an angular dependence in the case of the RS model, they do not noticeably alter the flat shape of the angular distribution for the pure scalar resonance exchange derived at leading order in QCD.

The angular analysis to discriminate the RS from the scalar model has been based on the center-edge asymmetry $A_{\rm CE}$, also estimated at NLO in QCD, for both the 14 TeV and the 7 TeV LHC. The numerical results for the predicted total number of resonant events and the minimum number of events for RS identification, obtained by the simple statistical arguments outlined in the previous section, are presented in Figs. 12 and 13 and summarized in Table I.

As regards the 7 TeV LHC, the theoretical results obtained above show that, taking into account recent experimental limits on the RS graviton mass, for luminosity around 10 fb^{-1} there may still be the possibility to identify the RS graviton excitation, in a rather limited range of M_G and small c. Higher luminosity, and/or larger LHC energy,

TABLE I. Theoretical discovery (5σ level) and 95% CL identification limits (NLO) on M_G in TeV. Excluded: identification not possible due to experimental bounds (Fig. 13—right panel).

$\sqrt{s}$, $\mathcal{L}_{\rm int}$	14 TeV, 100 fb^{-1}		7 TeV, 10 fb^{-1}	
$k/\bar{M}_{\rm Pl}$	Discovery	ID	Discovery	ID
0.01	2.6	2.0	1.2	~0.9
0.05	3.8	2.9	1.8	1.4
0.1	4.2	3.2	2.0	Excluded

would be required to extend this region by the A_{CE}-based angular analysis.

Finally, one may observe that the results regarding the RS graviton identification obtained in the previous section show that the inclusive diphoton process (1) at the LHC is complementary to the Drell-Yan dilepton production, in the sense that only the scalar exchange needs be considered as an alternative hypothesis for the source of resonance events. We have performed the A_{CE} angular analysis of the diphoton production cross sections for both hypotheses at NLO in QCD, and estimated numerical results for discovery and identification. The A_{CE} method has so far been applied to the dilepton channel at the LO in QCD only. Therefore, it should be interesting, for a fully exhaustive comparison of the results achievable from the two channels, to extend the A_{CE}-based angular analysis at NLO also to the dilepton production process.

ACKNOWLEDGMENTS

This research has been partially supported by funds of the University of Trieste and by the Abdus Salam ICTP under the TRIL and the Associates Programmes. P. M. acknowledges the ICTP for support. The work of M. C. K. and V. R. has been partially supported by the funds of Regional Center for Accelerator-based Particle Physics, Department of Atomic Energy, Government of India. We would also like to thank the cluster computing facility at Harish-Chandra Research Institute, where part of the computational work for this study was carried out. A conversation with I. A. Golutvin is gratefully acknowledged.

[1] L. Randall and R. Sundrum, Phys. Rev. Lett. **83**, 3370 (1999).
[2] H. Davoudiasl, J. L. Hewett, and T. G. Rizzo, Phys. Rev. D **63**, 075004 (2001); Phys. Rev. Lett. **84**, 2080 (2000).
[3] H. Davoudiasl and T. G. Rizzo, J. High Energy Phys. 11 (2008) 013.
[4] A. V. Kisselev, J. High Energy Phys. 09 (2008) 039.
[5] T. Aaltonen *et al.* (CDF Collaboration), Phys. Rev. D **83**, 011102 (2011).
[6] V. M. Abazov *et al.* (D0 Collaboration), Phys. Rev. Lett. **104**, 241802 (2010).
[7] ATLAS Collaboration, Report No. ATLAS-CONF-2011-044, 2011.
[8] See, for example, S. Esen (CMS Collaboration), arXiv:0910.3564.
[9] B. C. Allanach, K. Odagiri, M. A. Parker, and B. R. Webber, J. High Energy Phys. 09 (2000) 019.
[10] B. C. Allanach, K. Odagiri, M. J. Palmer, M. A. Parker, A. Sabetfakhri, and B. R. Webber, J. High Energy Phys. 12 (2002) 039.
[11] R. Cousins, J. Mumford, J. Tucker, and V. Valuev, J. High Energy Phys. 11 (2005) 046.
[12] A. Abulencia *et al.* (CDF Collaboration), Phys. Rev. Lett. **95**, 252001 (2005).
[13] P. Osland, A. A. Pankov, N. Paver, and A. V. Tsytrinov, Phys. Rev. D **78**, 035008 (2008).
[14] E. W. Dvergsnes, P. Osland, A. A. Pankov, and N. Paver, Int. J. Mod. Phys. A **20**, 2232 (2005).
[15] E. W. Dvergsnes, P. Osland, A. A. Pankov, and N. Paver, Phys. Rev. D **69**, 115001 (2004).
[16] R. Diener, S. Godfrey, and T. A. W. Martin, Phys. Rev. D **80**, 075014 (2009).
[17] U. De Sanctis, M. Fabbrichesi, and A. Tonero, Phys. Rev. D **84**, 015013 (2011).
[18] R. Kelley, L. Randall, and B. Shuve, J. High Energy Phys. 02 (2011) 014.
[19] C. W. Chiang, N. D. Christensen, G. J. Ding, and T. Han, arXiv:1107.5830 [Phys. Rev. D (to be published)].
[20] T. Han, J. D. Lykken, and R. J. Zhang, Phys. Rev. D **59**, 105006 (1999).
[21] L. D. Landau, Dokl. Akad. Nauk SSSR **60**, 207 (1948).
[22] C. N. Yang, Phys. Rev. **77**, 242 (1950).
[23] R. Barbieri and R. Torre, Phys. Lett. B **695**, 259 (2011).
[24] D. Feldman, Z. Liu, and P. Nath, J. High Energy Phys. 11 (2006) 007.
[25] J. Pumplin, D. R. Stump, J. Huston, H. L. Lai, P. M. Nadolsky, and W. K. Tung, J. High Energy Phys. 07 (2002) 012.
[26] S. Chatrchyan *et al.* (CMS Collaboration), J. High Energy Phys. 05 (2011) 093.
[27] T. Berger-Hryn'ova (ATLAS Collaboration), Proceedings of the International Europhysics Conference on High Energy Physics (EPS-HEP 2011), Grenoble, France; J. Abdallah (ATLAS Collaboration), Proceedings of the 19th International Conference on Particles and Nuclei (PANIC 11), Cambridge, MA, USA; see also ATLAS Collaboration, arXiv:1108.1582 [Phys. Rev. Lett. (to be published)].
[28] J. Tucker (CMS Collaboration), Proceedings of the International Europhysics Conference on High Energy Physics (EPS-HEP 2011), Grenoble, France; see also CMS Collaboration, CMS Physics Analysis Summary, Report No. CMS PAS EXO-11-019 and CMS Conference Report No. CMS CR-2011/255.
[29] O. J. P. Eboli, T. Han, M. B. Magro, and P. G. Mercadante, Phys. Rev. D **61**, 094007 (2000).
[30] G. F. Giudice, R. Rattazzi, and J. D. Wells, Nucl. Phys. **B544**, 3 (1999).
[31] K. m. Cheung and G. L. Landsberg, Phys. Rev. D **62**, 076003 (2000); K. m. Cheung, Phys. Rev. D **61**, 015005 (1999).

[32] K. Sridhar, J. High Energy Phys. 05 (2001) 066.
[33] G. F. Giudice, T. Plehn, and A. Strumia, Nucl. Phys. **B706**, 455 (2005).
[34] S. Chatrchyan *et al.* (CMS Collaboration), J. High Energy Phys. 05 (2011) 085.
[35] S. Frixione, Phys. Lett. B **429**, 369 (1998).
[36] P. Mathews, V. Ravindran, K. Sridhar, and W. L. van Neerven, Nucl. Phys. **B713**, 333 (2005).
[37] P. Mathews, V. Ravindran, and K. Sridhar, J. High Energy Phys. 10 (2005) 031.
[38] P. Mathews and V. Ravindran, Nucl. Phys. **B753**, 1 (2006).
[39] M. C. Kumar, P. Mathews, V. Ravindran, and A. Tripathi, Nucl. Phys. **B818**, 28 (2009).
[40] M. C. Kumar, P. Mathews, V. Ravindran, and A. Tripathi, Phys. Lett. B **672**, 45 (2009).
[41] B. W. Harris and J. F. Owens, Phys. Rev. D **65**, 094032 (2002).
[42] J. M. Campbell, R. K. Ellis, and C. Williams, J. High Energy Phys. 07 (2011) 018.
[43] G. Passarino and M. J. G. Veltman, Nucl. Phys. **B160**, 151 (1979).
[44] D. Graudenz, M. Spira, and P. M. Zerwas, Phys. Rev. Lett. **70**, 1372 (1993).
[45] A. Djouadi, M. Spira, and P. M. Zerwas, Phys. Lett. B **264**, 440 (1991).
[46] S. Dawson, Nucl. Phys. **B359**, 283 (1991).